Enhancement of voltage-controlled magnetic anisotropy through precise control of Mg insertion thickness at CoFeB|MgO interface

Xiang Li,[1,a)] Kevin Fitzell,[2,a)] Di Wu,[1,3] C. Ty Karaba,[4] Abraham Buditama,[4] Guoqiang Yu,[1] Kin L. Wong,[1] Nicholas Altieri,[2] Cecile Grezes,[1] Nicholas Kioussis,[5] Sarah Tolbert,[4] Zongzhi Zhang,[3] Jane P. Chang,[2] Pedram Khalili Amiri,[1,6] and Kang L. Wang[1]
[1]*Department of Electrical Engineering, University of California, Los Angeles, California 90095, USA*
[2]*Department of Chemical and Biomolecular Engineering, University of California, Los Angeles, California 90095, USA*
[3]*Department of Optical Science and Engineering, Key Laboratory of Micro and Nano Photonic Structures (Ministry of Education), Fudan University, Shanghai 200433, China*
[4]*Department of Chemistry and Biochemistry, University of California, Los Angeles, California 90095, USA*
[5]*Department of Physics and Astronomy, California State University, Northridge, California 91330, USA*
[6]*Inston, Inc., Los Angeles, California 90095, USA*

(Received 5 December 2016; accepted 18 January 2017; published online 30 January 2017)

We studied the impact of different insertion layers (Ta, Pt, and Mg) at the CoFeB|MgO interface on voltage-controlled magnetic anisotropy (VCMA) effect and other magnetic properties. Inserting a very thin Mg layer of 0.1–0.3 nm yielded a VCMA coefficient of 100 fJ/V-m, more than 3 times higher than the average values of around 30 fJ/V-m reported in Ta|CoFeB|MgO-based structures. Ta and Pt insertion layers also showed a small improvement, yielding VCMA coefficients around 40 fJ/V-m. Electrical, magnetic, and X-ray diffraction results reveal that a Mg insertion layer of around 1.2 nm gives rise to the highest perpendicular magnetic anisotropy, saturation magnetization, as well as the best CoFe and MgO crystallinity. Other Mg insertion thicknesses give rise to either under- or over-oxidation of the CoFe|MgO interface; a strong over-oxidation of the CoFe layer leads to the maximum VCMA effect. These results show that precise control over the Mg insertion thickness and CoFe oxidation level at the CoFeB|MgO interface is crucial for the development of electric-field-controlled perpendicular magnetic tunnel junctions with low write voltage. *Published by AIP Publishing.* [http://dx.doi.org/10.1063/1.4975160]

In the past decade, CoFeB|MgO|CoFeB-based magnetic tunnel junctions (MTJs) have been at the core of spintronic memory research and development. For practical memory applications, large tunneling magnetoresistance (TMR), perpendicular magnetic anisotropy (PMA), and switching efficiency are desirable. The physics behind the TMR and PMA phenomena has been widely studied in the context of the CoFeB|MgO interface.[1–4]

Recently, the electric-field-induced writing of perpendicular CoFeB|MgO|CoFeB MTJ structures has shown great promise for high density, high-speed, and energy efficient memory.[5,6] This electric-field- or voltage-induced magnetization switching exploits the voltage-controlled magnetic anisotropy (VCMA) effect to temporarily change the orientation of the magnetic easy axis of the CoFeB free layer during writing operations, thereby resulting in precessional reversal of the magnetization. This use of voltage requires drastically less energy than spin transfer torque (STT) and reduces the size of access transistors, resulting in higher bit density.[4,7] Previous work has shown sub-nanosecond writing of perpendicular MTJs with voltages of approximately 2 V for VCMA coefficients near 30 fJ/V-m.[7,8] In order to reduce the write voltage below 0.6 V to be compatible with advanced CMOS transistors, a higher VCMA coefficient of at least 100 fJ/V-m will be required.

The VCMA effect, i.e., the modification of the PMA by an external electric field, is also closely linked with the CoFeB|MgO interface. *Ab initio* calculations[9,10] suggest that the application of an electric field, corresponding to charge accumulation/depletion at the CoFeB|MgO interface, modifies the occupation of the hybridized Fe/Co and O orbitals responsible for generating the PMA.[10,11] More recent *ab initio* calculations revealed that epitaxial strain at the CoFe|MgO interface can lead to non-linear electric-field dependences of PMA.[12,13] Experimentally, the VCMA effect is found to be independent of the CoFeB thickness,[14–16] which suggests that the VCMA effect indeed originates from the CoFeB|MgO interface. While previous works have explored various seed and capping layers,[15,17] as well as insulating materials[18,19] in the MTJ structure in order to enlarge the VCMA coefficient, direct modification of the ferromagnet|insulator interface may provide a deeper understanding of the underlying physics of the VCMA effect, as well as guidance to further enhance the VCMA coefficient.

Ab initio calculations in the past have investigated the impact of different oxidation levels at the Fe|MgO interface on the VCMA effect: over-oxidation, under-oxidation, and the ideal Fe|MgO interface.[20,21] The impact on the VCMA coefficient of various heavy metal insertion layers (Pd, Pt, and Au) at the Fe|MgO interface was also studied theoretically.[22] Experimentally, there have been few VCMA studies using insertion layers at the ferromagnet|insulator interface. Hf insertion at the CoFeB|MgO interface[23] shows a limited VCMA effect around 4 fJ/V-m. A VCMA coefficient of around 86 fJ/V-m has been demonstrated using Pd insertion at the Co|MgO

[a)]X. Li and K. Fitzell contributed equally to this work.

interface,[24] but it is not based on the typical CoFeB|MgO structure for magnetic memory. Previous works have demonstrated that a thin Mg interlayer can improve the MgO (001) texture and thus the TMR ratio, as well as the thermal stress stability of PMA.[25–27] However, the impact of Mg insertion on the VCMA effect is still missing. Hence, there is a need for experimental work studying the role of Mg and various heavy metal materials inserted at the standard CoFeB|MgO interface for increasing the VCMA effect.

In this paper, the effect of Ta, Pt, and Mg insertion layers at the CoFeB|MgO interface is investigated. The VCMA coefficient, interfacial PMA, and saturation magnetization are analyzed for different insertion layer materials of various thicknesses. A maximum VCMA coefficient of 100 fJ/V-m is demonstrated for a Mg insertion layer thickness of 0.1–0.3 nm. In order to understand the observed trend and origin of the enhancement of the VCMA effect, synchrotron-based grazing-incidence wide-angle X-ray scattering (GIWAXS) was used to investigate the crystallinity and texture of the films as a function of the various insertion material thicknesses.

Three different materials were inserted into the CoFeB|MgO interface using magnetron sputtering. The stack structure consists of Ta(5)|CoFeB(1)|X(t)|MgO(2.5)|Al_2O_3(5) deposited on a thermally oxidized Si substrate, where the numbers in parentheses represent the layer thicknesses in nm. The insertion layer X (Ta, Pt, or Mg) has a continuously changing (wedged) thickness in the range of 0.1–0.3 nm for Ta and Pt and 0.1–2.4 nm for Mg. All metallic layers were grown using DC sputtering, while the insulating layers were grown using RF sputtering. The stacks were annealed at 325 °C for 30 min *in situ* in the sputtering system with a base pressure lower than 10^{-7} Torr. Subsequently, the films were patterned into Hall bar devices by photolithography and dry etching. A 33 nm Al_2O_3 gate oxide was deposited using atomic layer deposition (ALD), and Cr/Au layers were fabricated as a top gate electrode. The dielectric constants of MgO and Al_2O_3 were assumed to be 10 and 7, respectively.[28,29] The dimensions of the Hall bars were 20 μm × 130 μm. All electrical measurements were done at room temperature. The saturation magnetization values were obtained via a superconducting quantum interference device (SQUID) magnetometer.

Fig. 1(a) shows the measured anomalous Hall resistance (R_{Hall}) as a function of the out-of-plane magnetic field (H_Z) for CoFeB|Ta|MgO-based films. For Ta insertion layers thinner than ~0.22 nm, the CoFeB layer has an out-of-plane easy axis; as the Ta insertion layer thickness increases beyond 0.22 nm, the magnetic easy axis of the CoFeB layer undergoes a gradual transition to in-plane. This trend also applies to the case of Pt and Mg insertion layers when the hard axis anisotropy fields (H_K) are plotted, as shown in Fig. 1(b). However, the insertion layer thickness at which this transition occurs is very thin in the cases of Ta and Pt (0.22 nm and 0.17 nm, respectively) and much thicker in the case of Mg (1.53 nm). Possible reasons for this difference in transition thickness will be discussed later. Note that, since PMA is strongly desired in these devices, investigation into insertion layers thicker than the transition thicknesses is not the primary goal of this work.

To extract the VCMA coefficient, the anomalous Hall effect (AHE) is used to characterize the perpendicular

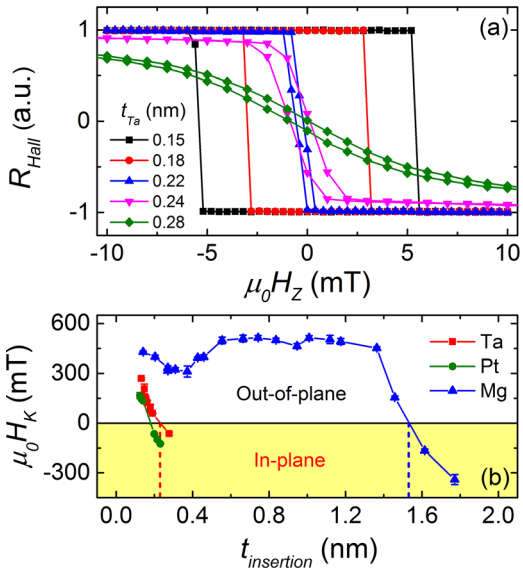

FIG. 1. (a) Anomalous Hall resistance (R_{Hall}) as a function of applied perpendicular magnetic field ($\mu_0 H_Z$) for different Ta insertion thicknesses (t_{Ta}). (b) Hard axis anisotropy field ($\mu_0 H_K$) as a function of insertion layer thickness ($t_{insertion}$) for Ta, Pt, and Mg. The region where $\mu_0 H_K > 0$ (<0) refers to that the CoFeB is out-of-plane (in-plane) easy axis.

anisotropy energy volume density (E_{perp}) under different gate voltages by sweeping the magnetic field along the hard axis of the CoFeB.[15,16,30] For perpendicular CoFeB, $E_{\mathrm{perp}} = \mu_0 M_S \int_0^1 H_X d(M_X/M_S)$, where the normalized in-plane magnetization, M_X/M_S, can be obtained through the normalized R_{Hall} values. The electric-field-dependent interfacial PMA values, K_i, can be obtained via $E_{\mathrm{perp}}(E) = K_i(E)/t_{CoFeB} - \mu_0 M_S^2/2$. The slope of K_i versus electric field equals the VCMA coefficient, ξ.

One result of using this method for an Mg insertion layer sample ($t_{Mg} = 0.31$ nm) is shown in Fig. 2(a). First, the anomalous Hall resistance dependence on the in-plane magnetic field is shown under various applied gate voltages. The inset in the upper right corner clearly shows the difference between the hard axis $R_{Hall} - \mu_0 H_X$ loops under three different gate voltages. The calculated values of K_i versus electric field are shown in Fig. 2(b). The linear fit gives a negative VCMA coefficient of −95.7 ± 2.7 fJ/V-m. Note that the K_i values were obtained by applying multiple back-and-forth gate voltage sweeps: 5 V to −5 V and back to 5 V, swept three times. The small linear fitting error indicates that there is minimal mobile ionic charge in our material stacks.[31,32]

Following the above method, the VCMA coefficient and interfacial PMA K_i were measured for various insertion materials with various thicknesses. The results are shown in Figs. 3(a) and 3(b). Note that all VCMA values are absolute values. For Ta and Pt insertions, the VCMA coefficients have maximum values in the range of 40–50 fJ/V-m. However, for the Mg insertion sample, the VCMA values show a large variation from almost zero to maximum values of around 100 fJ/V-m. Here, we will break down the range of Mg insertion thicknesses into four different regions: Region I, $0.1\ \mathrm{nm} < t_{Mg} < 0.3$ nm; Region II, $0.5\ \mathrm{nm} < t_{Mg} < 1.1$ nm; Region III, $1.1\ \mathrm{nm} < t_{Mg} < 1.3$ nm; and Region IV, $t_{Mg} > 1.3$ nm. Compared with published VCMA coefficients of around 30 fJ/V-m based on Ta|CoFeB|MgO structures,[30,33,34] the VCMA coefficients in

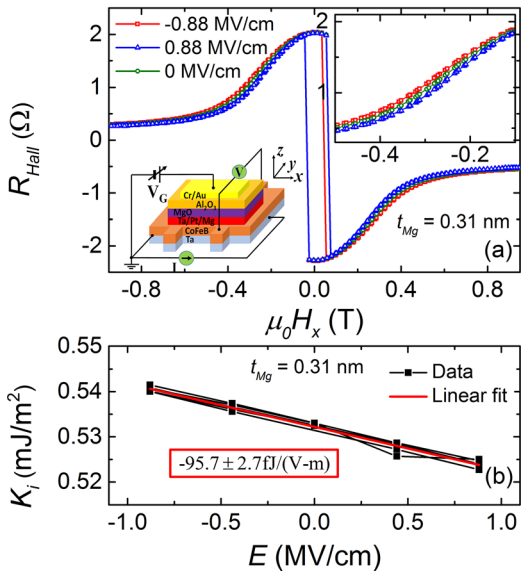

FIG. 2. (a) Hall resistance (R_{Hall}) as a function of in-plane magnetic field ($\mu_0 H_X$) under different applied gate electric fields (E). Top right inset: Zoomed-in view of R_{Hall} - $\mu_0 H_X$ data with $-0.5\,\mathrm{T} < \mu_0 H_X < -0.1\,\mathrm{T}$. Bottom left inset: Schematic for the Hall bar device under different applied gate voltages (V_G). A positive gate voltage is defined as the top gate electrode being at a positive electric potential, as shown in the bottom left inset. (b) Interfacial perpendicular magnetic anisotropy (K_i) as a function of E. The K_i values were obtained by applying multiple back-and-forth gate voltage sweeps: 5 V to −5 V and back to 5 V, for three times. The linear fit of the K_i values versus E yields a VCMA coefficient $\xi = -95.7 \pm 2.7$ fJ/(V-m). Data from (a) and (b) are obtained from a device with a Mg insertion layer thickness of 0.31 nm.

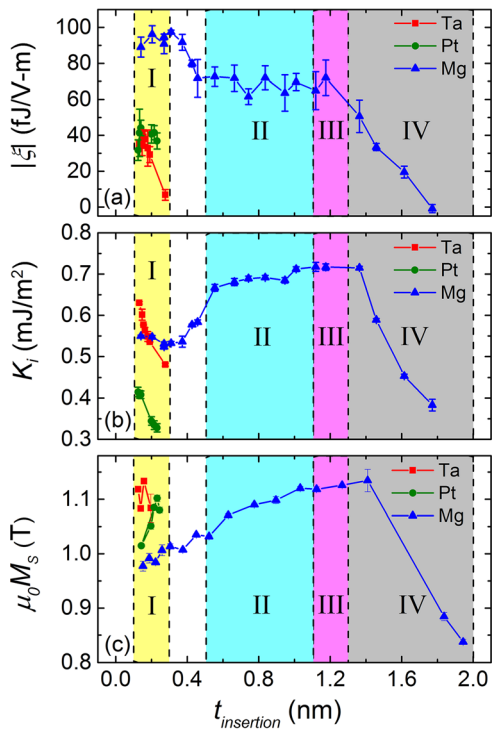

FIG. 3. (a) VCMA coefficient (ξ), (b) interfacial perpendicular magnetic anisotropy (K_i), and (c) saturation magnetization ($\mu_0 M_S$) as a function of insertion layer thickness ($t_{insertion}$) for Ta, Pt, and Mg. The VCMA coefficients here are all absolute values, while the measured values are all negative (according to the definition that positive voltage corresponds to higher electric potential at the top gate electrode). Regions I–IV are designated with different colors.

Region I are improved by more than a factor of 3. The VCMA coefficients first decrease and then reach a plateau from Region I to Regions II and III. With further increase of the Mg thickness to Region IV, the VCMA coefficient drastically approaches zero. Interfacial PMA (K_i) values decrease for Ta and Pt at thicker insertion thicknesses. For Mg, the K_i dependence on Mg insertion layer thickness is non-monotonic. In Region III, where the VCMA plateaus around 70 fJ/V-m, the PMA reaches maximum. The PMA first sharply decreases and then increases slightly when t_{Mg} transitions from Region II to I. In Region IV, both VCMA and PMA decrease sharply.

The saturation magnetization (M_S) dependences on insertion material thickness for all three materials (Ta, Pt, and Mg) are shown in Fig. 3(c). The saturation magnetization values of all three materials peak around 1.1 T. Interestingly, the peak of the M_S values for Mg is around 1.2 nm (Region III), where the PMA reaches maximum. For thicknesses less than 1.2 nm, M_S decreases gradually, while for Mg thickness larger than 1.2 nm, M_S decreases sharply. Note that all saturation magnetization values here were obtained without considering any CoFeB dead layer.

First, we will analyze the case of Mg insertion in detail before comparing it against Ta/Pt insertions. We hypothesize that the change of CoFe oxidation levels with varying Mg insertion thicknesses contributes to the above observed VCMA, PMA, and M_S dependence on the Mg insertion thickness. Here, the oxygen content responsible for oxidizing CoFe partly comes from the high energy O^- ions generated in the RF sputtering of MgO, which will bombard and oxidize the CoFeB|Mg layers underneath.[35–37] In addition, during the post annealing process, oxygen from the MgO and Al_2O_3 layers might diffuse into the CoFeB|Mg layers.[38] Thus, using a Mg insertion layer of an appropriate thickness can precisely control the oxidation level of the CoFeB layer. In particular, our hypothesis is that Region III corresponds to an ideal CoFe|MgO interface, Regions I and II to an over-oxidized CoFe|MgO interface (Co/Fe-oxides at the interface), and Region IV to an under-oxidized CoFe|MgO interface (metallic Mg at the interface).

To validate this hypothesis, X-ray diffraction (XRD) studies on the unpatterned film stacks were performed at the Stanford Synchrotron Radiation Lightsource (SSRL) using the 11–3 beamline, which is specially equipped for grazing incidence wide angle X-ray scattering (GIWAXS). Two-dimensional XRD patterns, which contain information on the phase, stress, texture, and grain size of the samples, were obtained for various Mg insertion layer thicknesses and integrated over a small range of azimuthal angle χ in the 2D scan. Two sets of data are obtained for different Mg insertion thicknesses as shown in Figs. 4(a) and 4(b) as a function of different q values while integrating over a range of χ values. As highlighted in Figs. 4(a) and 4(b), CoFe (110) and MgO (220) crystalline peaks only show up prominently for a Mg insertion layer thickness of 1.20 nm. This thickness range near 1.20 nm corresponds to Region III, where the PMA and M_S are also the highest as seen from Figs. 3(b) and 3(c). Fig. 4(a) shows a broad peak at q values from 2.4 to 2.8 A^{-1}, which we attribute to a convolution of amorphous and/or small crystallite signals from Ta, Al_2O_3, SiO_2, and possibly $CoFe_2O_4$. Unfortunately, the large number of overlapping

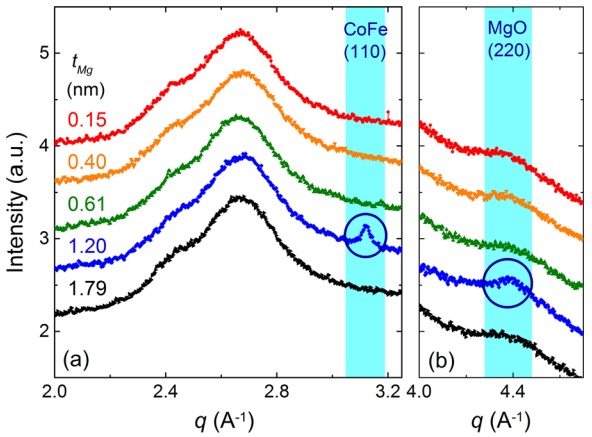

FIG. 4. X-ray diffraction (XRD) intensity versus reciprocal lattice vector q for films with different Mg insertion layer thicknesses (t_{Mg}). (a) The data are integrated over azimuthal angle χ at $80° < \chi < 100°$. The q value region corresponding to the crystalline peak for CoFe (110) is highlighted. (b) The data are integrated over azimuthal angle χ at $40° < \chi < 80°$. The q value region corresponding to the crystalline peak for MgO (220) is highlighted.

peaks in this region prevented a quantitative analysis of each material as a function of the insertion layer thickness. From the peak positions of CoFe and MgO, we can calculate that there is a 3%–4% lattice mismatch between CoFe and MgO, which is consistent with published results.[39]

The above observation that the crystalline CoFe and MgO peaks only show up prominently in Region III corroborates our hypothesis that only Region III corresponds to an ideal CoFe|MgO interface. This can be explained by considering the crystallization process of CoFeB in the CoFeB|MgO material system. It is widely accepted that the MgO becomes crystalline when deposited onto amorphous CoFeB and that the CoFeB crystalizes based on the crystallinity of the adjacent MgO layer.[39,40] In other words, if the CoFe|MgO interface is under-oxidized, the excessive Mg interlayer between CoFe and MgO may prevent the formation of crystalline MgO during deposition, as well as the crystallization of CoFeB based on the MgO crystal orientation. On the other hand, if the CoFe|MgO interface is over-oxidized, the Co/Fe-oxides will also degrade the CoFeB crystallization quality. In the following discussion, we will explain the VCMA, PMA, and M_S dependence on the Mg insertion thickness using this corroborated hypothesis.

In order to understand why the maximum M_S value shows up in Region III, the effect of CoFeB oxidation on the magnetic properties of the layered system must be considered. Generally, it is known that CoFe oxidizes into either an antiferromagnetic (CoO, FeO, α-Fe_2O_3)[41] or ferrimagnetic (Fe_3O_4, γ-Fe_2O_3, $CoFe_2O_4$) phase, all of which have lower M_S values than Co and Fe.[42] Thus, for Mg thickness smaller than Region III, the thinner the Mg is, the more CoFeB will be oxidized, resulting in a lower M_S value. This lower M_S value may also be caused by the sputtering effect of CoFeB|Mg layers during MgO deposition.[43] In addition, the CoFeB crystallization quality thus the M_S value is lower for Mg thickness thicker than Region III too.[44]

The thickness of the Mg insertion layer also exhibits a complex effect on the PMA of CoFeB. *Ab initio* calculations have shown that an under-oxidized CoFe|MgO interface will lead to a decrease in PMA due to the disappearance of Fe/Co - O hybridized states compared to an ideal CoFe|MgO interface, while an over-oxidized CoFe|MgO interface leads to a decrease in PMA as a result of the splitting of these same hybridized states.[11,45] Other experimental work also shows similar results.[46–48] Generally, the PMA decreases for Mg insertion layer thicknesses other than Region III. However, the PMA of the CoFeB shows a small increase when a very thin Mg insertion layer is inserted (Region I). This might be attributed to different strain conditions[49] at the over-oxidized CoFe|MgO interface as well as the formation of $CoFe_2O_4$.[50]

Lastly, the effect of the Mg insertion layer thickness on the VCMA magnitude will be discussed. Our results suggest that a strongly over-oxidized CoFe|MgO interface will increase the VCMA effect. This observed trend is also consistent with *ab initio* calculations where an interfacial FeO layer enhanced the VCMA coefficient.[20,21] A deeper understanding of the evolution of the VCMA effect from the very thin Mg insertion thickness (Region I) to the Mg insertion thickness showing an ideal CoFe|MgO interface (Region III) requires *ab initio* calculations, which also take into account the different strain conditions when the CoFe|MgO interface are under different oxidation levels.[12,13]

After understanding the case of Mg insertion, Ta and Pt insertion layers will be discussed briefly as a comparison. First, as can be seen from both Figs. 1 and Fig. 3(b), the PMA decreases with increasing Ta/Pt/Mg insertion thickness, consistent with previous reports.[27,51] As shown in Fig. 1(b), a Mg insertion layer induces a much larger out-of-plane to in-plane transition thickness than Ta/Pt. One cause for this difference in transition thickness might be that as the PMA originates from the hybridization of Co/Fe and O orbitals at the CoFeB|MgO interface,[10,11] a sufficiently thick extrinsic insertion layer, such as Ta or Pt, will weaken the Co/Fe and O orbitals hybridization by binding to the O atoms, thus leading to the decrease of PMA.[52] Second, as the VCMA effect is the modulation of PMA, the decreased extent of Co/Fe and O orbitals hybridization might also decrease the VCMA effect, as shown in Fig. 3(a). Third, at very small insertion thicknesses, the M_S values for Ta/Pt insertions are much larger than that of the Mg, as shown in Fig. 3(c). This difference could be understood by considering that Ta/Pt has a smaller negative oxide formation enthalpy than Mg. Hence, during the MgO deposition and annealing processes, the lower degree of CoFeB oxidation for the Ta/Pt insertion scenario might result in a higher M_S. Another possible reason is that the MgO deposition process will also sputter the CoFeB and metallic insertion layers underneath.[43] With larger atomic numbers and higher sublimation temperatures than Mg, the Ta and Pt insertion layers are harder to be sputtered off. Therefore, less CoFeB is sputtered off and a larger M_S is obtained.

In conclusion, we systematically studied how inserting various materials (Ta, Pt, and Mg) at the CoFeB|MgO interface affects the VCMA effect. A maximum VCMA coefficient of around 100 fJ/V-m was realized for a very thin Mg insertion layer, which is more than 3 times larger compared to average VCMA values reported for traditional CoFeB|MgO stacks where no material is inserted. Using XRD results, the emergence of strong CoFe and MgO crystalline peaks is correlated with the maximum PMA and saturation magnetization. This

indicates that precise control over the Mg insertion thickness and CoFe oxidation level at the CoFeB|MgO interface is critical to achieving the desired device performance, with a trade-off between VCMA, PMA, and saturation magnetization. The high VCMA coefficient of around 100 fJ/V-m demonstrated in this work will pave the way for low-power high-density magnetoelectric memories utilizing electric-field-induced writing with very low write voltage.

This work was partially supported by the NSF Nanosystems Engineering Research Center for Translational Applications of Nanoscale Multiferroic Systems (TANMS). The work at Inston was supported in part by a Phase II NSF Small Business Innovation Research award. This work was supported in part by C-SPIN and FAME, two of six centers of STARnet, a Semiconductor Research Corporation program, sponsored by MARCO and DARPA. We would like to acknowledge the collaboration of this research with the King Abdul-Aziz City for Science and Technology (KACST) via The Center of Excellence for Green Nanotechnologies (CEGN). This work was partially supported by the Energy Frontier Research Center for Spins and Heat in Nanoscale Electronic Systems (SHINES). D. Wu and Z. Z. Zhang thank the support of China Scholarship Council (CSC), the 973 Program (2014CB921104), and the NSFC Grant No. 11474067. The authors would also like to acknowledge fruitful discussions with Patrick Yee, Greg Carman, and Dana Cairns Watson.

[1]J. Y. Bae, W. C. Lim, H. J. Kim, T. D. Lee, K. W. Kim, and T. W. Kim, J. Appl. Phys. **99**(8), 08T316 (2006).
[2]S. Ikeda, J. Hayakawa, Y. Ashizawa, Y. M. Lee, K. Miura, H. Hasegawa, M. Tsunoda, F. Matsukura, and H. Ohno, Appl. Phys. Lett. **93**(8), 082508 (2008).
[3]N. Miyakawa, D. C. Worledge, and K. Kita, IEEE Magn. Lett. **4**, 1000104 (2013).
[4]P. K. Amiri, Z. M. Zeng, J. Langer, H. Zhao, G. Rowlands, Y. J. Chen, I. N. Krivorotov, J. P. Wang, H. W. Jiang, J. A. Katine, Y. Huai, K. Galatsis, and K. L. Wang, Appl. Phys. Lett. **98**(11), 112507 (2011).
[5]W. G. Wang, M. Li, S. Hageman, and C. L. Chien, Nat. Mater. **11**(1), 64 (2012).
[6]Y. Shiota, T. Nozaki, F. Bonell, S. Murakami, T. Shinjo, and Y. Suzuki, Nat. Mater. **11**(1), 39 (2012).
[7]C. Grezes, F. Ebrahimi, J. G. Alzate, X. Cai, J. A. Katine, J. Langer, B. Ocker, P. K. Amiri, and K. L. Wang, Appl. Phys. Lett. **108**(1), 012403 (2016).
[8]S. Kanai, F. Matsukura, and H. Ohno, Appl. Phys. Lett. **108**(19), 192406 (2016).
[9]M. K. Niranjan, C.-G. Duan, S. S. Jaswal, and E. Y. Tsymbal, Appl. Phys. Lett. **96**(22), 222504 (2010).
[10]K. H. He, J. S. Chen, and Y. P. Feng, Appl. Phys. Lett. **99**(7), 072503 (2011).
[11]H. X. Yang, M. Chshiev, B. Dieny, J. H. Lee, A. Manchon, and K. H. Shin, Phys. Rev. B **84**(5), 054401 (2011).
[12]P. V. Ong, N. Kioussis, D. Odkhuu, P. K. Amiri, K. L. Wang, and G. P. Carman, Phys. Rev. B **92**(2), 020407 (2015).
[13]P. V. Ong, N. Kioussis, P. K. Amiri, and K. L. Wang, Sci. Rep. **6**, 29815 (2016).
[14]A. Okada, S. Kanai, M. Yamanouchi, S. Ikeda, F. Matsukura, and H. Ohno, Appl. Phys. Lett. **105**(5), 052415 (2014).
[15]X. Li, G. Yu, H. Wu, P. V. Ong, K. Wong, Q. Hu, F. Ebrahimi, P. Upadhyaya, M. Akyol, N. Kioussis, X. Han, P. K. Amiri, and K. L. Wang, Appl. Phys. Lett. **107**(14), 142403 (2015).
[16]X. Li, M.S. dissertation, UCLA: Electrical Engineering 0303 (2015).
[17]W. Skowroński, T. Nozaki, D. D. Lam, Y. Shiota, K. Yakushiji, H. Kubota, A. Fukushima, S. Yuasa, and Y. Suzuki, Phys. Rev. B **91**(18), 184410 (2015).
[18]K. Kita, D. W. Abraham, M. J. Gajek, and D. C. Worledge, J. Appl. Phys. **112**(3), 033919 (2012).
[19]D. Chien, X. Li, K. Wong, M. A. Zurbuchen, S. Robbennolt, G. Yu, S. Tolbert, N. Kioussis, P. K. Amiri, K. L. Wang, and J. P. Chang, Appl. Phys. Lett. **108**(11), 112402 (2016).
[20]K. Nakamura, T. Akiyama, T. Ito, M. Weinert, and A. J. Freeman, Phys. Rev. B **81**(22), 220409(R) (2010).
[21]F. Ibrahim, A. Hallal, B. Dieny, and M. Chshiev, e-print arXiv:1610.08859.
[22]M. Tsujikawa, S. Haraguchi, and T. Oda, J. Appl. Phys. **111**(8), 083910 (2012).
[23]T. Bonaedy, J. W. Choi, C. Jang, B.-C. Min, and J. Chang, J. Phys. D: Appl. Phys. **48**(22), 225002 (2015).
[24]H. Yuki, K. Tomohiro, O. Aya, M. Kazumoto, O. Shimpei, and C. Daichi, Appl. Phys. Express **8**(11), 113002 (2015).
[25]G.-X. Miao, K. B. Chetry, A. Gupta, W. H. Butler, K. Tsunekawa, D. Djayaprawira, and G. Xiao, J. Appl. Phys. **99**(8), 08T305 (2006).
[26]Y. Lu, C. Deranlot, A. Vaurès, F. Petroff, J. M. George, Y. Zheng, and D. Demailles, Appl. Phys. Lett. **91**(22), 222504 (2007).
[27]Q. L. Ma, S. Iihama, T. Kubota, X. M. Zhang, S. Mizukami, Y. Ando, and T. Miyazaki, Appl. Phys. Lett. **101**(12), 122414 (2012).
[28]J. Robertson, Eur. Phys. J. Appl. Phys. **28**(3), 265 (2004).
[29]M. D. Groner, J. W. Elam, F. H. Fabreguette, and S. M. George, Thin Solid Films **413**(1–2), 186 (2002).
[30]M. Endo, S. Kanai, S. Ikeda, F. Matsukura, and H. Ohno, Appl. Phys. Lett. **96**(21), 212503 (2010).
[31]T. Maruyama, Y. Shiota, T. Nozaki, K. Ohta, N. Toda, M. Mizuguchi, A. A. Tulapurkar, T. Shinjo, M. Shiraishi, S. Mizukami, Y. Ando, and Y. Suzuki, Nat. Nanotechnol. **4**(3), 158 (2009).
[32]U. Bauer, M. Przybylski, J. Kirschner, and G. S. Beach, Nano Lett. **12**(3), 1437 (2012).
[33]Y. Shiota, F. Bonell, S. Miwa, N. Mizuochi, T. Shinjo, and Y. Suzuki, Appl. Phys. Lett. **103**(8), 082410 (2013).
[34]J. Zhu, J. A. Katine, G. E. Rowlands, Y.-J. Chen, Z. Duan, J. G. Alzate, P. Upadhyaya, J. Langer, P. K. Amiri, K. L. Wang, and I. N. Krivorotov, Phys. Rev. Lett. **108**(19), 197203 (2012).
[35]K. Ono, N. Ohshima, K. Goto, H. Yamamoto, T. Morita, K. Kinoshita, T. Ishijima, and H. Toyoda, Jpn. J. Appl. Phys. **50**(2), 023001 (2011).
[36]H. Toyoda, K. Goto, T. Ishijima, T. Morita, N. Ohshima, and K. Kinoshita, Appl. Phys. Express **2**(12), 126001 (2009).
[37]T. Ishijima, K. Goto, N. Ohshima, K. Kinoshita, and H. Toyoda, Jpn. J. Appl. Phys. **48**(11), 116004 (2009).
[38]X. Qiu, K. Narayanapillai, Y. Wu, P. Deorani, D.-H. Yang, W.-S. Noh, J.-H. Park, K.-J. Lee, H.-W. Lee, and H. Yang, Nat. Nanotechnol. **10**(4), 333 (2015).
[39]Y. S. Choi, K. Tsunekawa, Y. Nagamine, and D. Djayaprawira, J. Appl. Phys. **101**(1), 013907 (2007).
[40]S. Yuasa, Y. Suzuki, T. Katayama, and K. Ando, Appl. Phys. Lett. **87**(24), 242503 (2005).
[41]B. D. Cullity and C. D. Graham, *Introduction to Magnetic Materials* (John Wiley & Sons, Inc., 2008), pp. 115.
[42]H. M. Lu, W. T. Zheng, and Q. Jiang, J. Phys. D: Appl. Phys. **40**(2), 320 (2007).
[43]J. Swerts, S. Mertens, T. Lin, S. Couet, Y. Tomczak, K. Sankaran, G. Pourtois, W. Kim, J. Meersschaut, L. Souriau, D. Radisic, S. Van Elshocht, G. Kar, and A. Furnemont, Appl. Phys. Lett. **106**(26), 262407 (2015).
[44]T. Liu, Y. Zhang, J. W. Cai, and H. Y. Pan, Sci Rep. **4**, 5895 (2014).
[45]W. Kim, J. H. Jeong, Y. Kim, W. C. Lim, J. H. Kim, J. H. Park, H. J. Shin, Y. S. Park, K. S. Kim, S. H. Park, Y. J. Lee, K. W. Kim, H. J. Kwon, H. L. Park, H. S. Ahn, S. C. Oh, J. E. Lee, S. O. Park, S. Choi, H. K. Kang, and C. Chung, in 2011 IEEE International Electron Devices Meeting (IEDM) (2011).
[46]L. E. Nistor, B. Rodmacq, C. Ducruet, C. Portemont, I. L. Prejbeanu, and B. Dieny, IEEE Trans. Magn. **46**(6), 1412 (2010).
[47]W. C. Tsai, S. C. Liao, H. C. Hou, C. T. Yen, Y. H. Wang, H. M. Tsai, F. H. Chang, H. J. Lin, and C.-H. Lai, Appl. Phys. Lett. **100**(17), 172414 (2012).
[48]N. Sato, A. El-Ghazaly, R. M. White, and S. X. Wang, IEEE Trans. Magn. **52**(7), 1400304 (2016).
[49]P. V. Ong, N. Kioussis, P. K. Amiri, K. L. Wang, and G. P. Carman, J. Appl. Phys. **117**(17), 17B518 (2015).
[50]A. Lisfi, C. M. Williams, L. T. Nguyen, J. C. Lodder, A. Coleman, H. Corcoran, A. Johnson, P. Chang, A. Kumar, and W. Morgan, Phys. Rev. B **76**(5), 054405 (2007).
[51]G. Yu, P. Upadhyaya, X. Li, W. Li, S. K. Kim, Y. Fan, K. L. Wong, Y. Tserkovnyak, P. K. Amiri, and K. L. Wang, Nano Lett. **16**(3), 1981 (2016).
[52]G. Yu, L.-T. Chang, M. Akyol, P. Upadhyaya, C. He, X. Li, K. L. Wong, P. K. Amiri, and K. L. Wang, Appl. Phys. Lett. **105**(10), 102411 (2014).